Applied Physics Letters

NbTiN thin films for superconducting photon detectors on photonic and two-dimensional materials

Cite as: Appl. Phys. Lett. **116**, 171101 (2020); https://doi.org/10.1063/1.5143986
Submitted: 28 December 2019 . Accepted: 09 April 2020 . Published Online: 27 April 2020

Stephan Steinhauer, Lily Yang, Samuel Gyger, Thomas Lettner, Carlos Errando-Herranz, Klaus D. Jöns, Mohammad Amin Baghban, Katia Gallo, Julien Zichi, and Val Zwiller

Applied Physics Letters ARTICLE scitation.org/journal/apl

NbTiN thin films for superconducting photon detectors on photonic and two-dimensional materials

Cite as: Appl. Phys. Lett. **116**, 171101 (2020); doi: 10.1063/1.5143986
Submitted: 28 December 2019 · Accepted: 9 April 2020 ·
Published Online: 27 April 2020

View Online Export Citation CrossMark

Stephan Steinhauer,[a] Lily Yang, Samuel Gyger, Thomas Lettner, Carlos Errando-Herranz, Klaus D. Jöns, Mohammad Amin Baghban, Katia Gallo, Julien Zichi, and Val Zwiller[b]

AFFILIATIONS

Department of Applied Physics, KTH Royal Institute of Technology, SE-106 91 Stockholm, Sweden

[a]Author to whom correspondence should be addressed: ssteinh@kth.se
[b]Electronic mail: zwiller@kth.se

ABSTRACT

Integration of superconducting devices on photonic platforms opens up a wide range of functionalities and applications. We report on NbTiN thin films deposited on SiO_2, Si_3N_4, GaAs, $LiNbO_3$, and AlN as well as on a monolayer of hexagonal boron nitride, using a universal reactive co-sputtering recipe. The morphology and the superconducting properties of the NbTiN thin films with a thickness of 10 nm were characterized by atomic force microscopy and electrical transport measurements. Superconducting strip photon detectors were fabricated using a design suitable for waveguide integration and compared in terms of their internal quantum efficiency and detection pulse kinetics. Our results show well-comparable performances for detectors integrated on different platforms, while also demonstrating that reactive co-sputter deposition of NbTiN at room temperature provides a robust method for realizing superconducting devices on various materials.

Superconducting materials are the fundamental building block for a wide variety of devices such as Josephson junctions, magnetic field probes, and electromagnetic radiation detectors. Moreover, they form a platform for quantum computing as well as neuromorphic circuit architectures. To utilize the full potential of superconducting thin films and take advantage of their versatile functionalities, fabrication processes suitable for integration on different platforms are required. For instance, superconducting strip photon detectors[1] (SSPDs; nomenclature according to the International Standard IEC is used,[2] whereas in the literature, these devices are also referred to as superconducting nanowire single-photon detectors) have been demonstrated with different thin film systems on multiple substrate materials and have evolved into the leading technology for single-photon detection.[3,4] They offer a wide wavelength sensitivity range,[5] high detection efficiency, low dark count rate, and high time resolution[6–9] and can be integrated on waveguides in photonic integrated circuits.[10] However, integration of SSPDs is often complicated by application-specific restrictions and dedicated growth processes using high temperatures or intermediate buffer layers. While amorphous materials such as WSi are associated with high detection efficiencies and a forgiving fabrication process resulting in a good detector fabrication yield,[11] it is challenging to achieve low timing jitter[12] and detector operation typically requires sub-Kelvin temperatures. On the other hand, the nitride-based superconductors NbN and NbTiN excel in time resolution but are less forgiving in terms of fabrication yield due to their nanocrystalline structure, often requiring deposition at elevated temperatures.

In this Letter, we show the integration of NbTiN-based SSPD devices on photonic and monolayer two-dimensional materials using a universal reactive co-sputtering process at room temperature. Six substrate materials were studied: silicon dioxide (SiO_2), silicon nitride (Si_3N_4), gallium arsenide (GaAs), lithium niobate ($LiNbO_3$), aluminum nitride (AlN), and hexagonal boron nitride (hBN). SiO_2 is commonly used for the fabrication of free-space or fiber-coupled SSPDs due to the refractive index difference between SiO_2 and the Si substrate underneath forming a weak optical cavity.[13] Si_3N_4 is a CMOS-compatible material that offers a wide transparency window from the visible to the mid-infrared and is suitable for efficient photonic waveguiding. SSPDs can be integrated either before Si_3N_4 growth as embedded detectors[14] or on top of the photonic circuit.[15] AlN is used as a piezo-electric material, for instance, in resonators, transducers, and actuators. Superconducting detectors were also fabricated using a pick and place technique[16] and by NbN deposition at high temperatures.[17] $LiNbO_3$ as an optically non-linear material with a large transparency window and electro-optical properties allows for second-harmonic generation and electro-optic modulation. SSPDs were demonstrated on planar substrates,[18,19] whereas superconducting transition-edge sensors were realized on titanium in-diffused waveguides.[20] GaAs is a common photonic platform that also allows for the fabrication of quantum dot-based non-classical light sources. The integration of NbN SSPDs requires precise control of deposition temperature to preserve the substrate integrity[21–23] or the use of a buffer layer.[24] Finally, two-dimensional crystals and van der Waals heterostructures have emerged as optoelectronic platforms with unique characteristics.[25] hBN, in particular, is an important building block that is used as a dielectric, for passivation or for its optical properties in the ultraviolet range.[26] However, SSPDs realized on two-dimensional crystals as substrate material have remained unexplored so far.

We realized NbTiN thin films by reactive co-sputtering from separate Nb and Ti targets at room temperature. We developed a universal recipe for the deposition of 10 nm NbTiN on all six material platforms without substrate-dependent adaptation. The deposition rate and nominal film thickness were monitored *in situ* using a rate monitor calibrated for SiO_2/Si substrates (uncertainty 5%). The magnetron sources were operated at a DC bias of 120 W and a RF bias of 240 W for Nb and Ti, respectively, using an Ar/N_2 ratio of 10 and a sputtering pressure of 3 mTorr. These deposition conditions result in polycrystalline films with a Nb/Ti ratio around 60% suitable for high-efficiency SSPDs with a sub-20 ps timing jitter, as reported previously for SiO_2/Si substrates.[27] The following samples were used: thin film SiO_2 on Si (150 nm thermal oxide), thin film Si_3N_4 on SiO_2/Si (250 nm low pressure chemical vapor deposition; Rogue Valley Microdevices), bulk GaAs wafer (Wafer Technology); bulk $LiNbO_3$ wafer (x-cut; CasTech), thin film AlN on Si (200 nm plasma vapor deposition; Kyma Technologies), and monolayer hBN on SiO_2/Si (chemical vapor deposition growth and PMMA transfer, oxide thickness 285 nm; Graphene Supermarket). Measurements of NbTiN step heights by atomic force microscopy in tapping mode suggested well-comparable thicknesses for films on SiO_2 compared to Si_3N_4, GaAs, $LiNbO_3$, and AlN with relative differences below 4% (hBN was excluded from the step height analysis due to surface irregularities resulting from the transfer process). Furthermore, the surface morphology of all substrates was assessed (Fig. 1), characterizing areas with NbTiN as well as bare substrate areas covered during the deposition. The root mean square surface roughness R_q was extracted and is summarized for all the cases in Table I. Sputtering of 10 nm NbTiN at room temperature had a negligible influence on the surface roughness, confirming the homogeneity of film deposition. Low R_q values of 0.3–0.6 nm were found for SiO_2, Si_3N_4, and GaAs, whereas larger values were measured for $LiNbO_3$ (0.9 nm), hBN (1.0 nm), and AlN (1.2 nm). In the latter case of AlN, the surface roughness was determined by its distinct grain morphology [Fig. 1(e)]. Note that for the monolayer hBN substrate, circular surface irregularities were present, which were excluded from the roughness analysis.

The electrical properties of the NbTiN thin films on all six material platforms were extracted from measurements in a custom cryogenic setup, in particular, the room temperature sheet resistance R_{sh}, the critical temperature T_c (temperature at which the resistance is equal to half of that at 20 K), the residual resistance ratio *RRR* (ratio of the resistance at 300 K over that at 20 K), and the superconducting transition width ΔT_c (difference between the temperatures corresponding to 10% and 90% of the resistance at 20 K). The results for these four parameters are summarized in Table I. Similar T_c values between 10.1 K (hBN) and 11.0 K (AlN) were observed without relying on substrate-dependent optimization of deposition. We expect that the crystalline structure of AlN impacts the NbTiN growth due to improved lattice matching conditions,[28] resulting in increased T_c. Similar parameters were also found for R_{sh} (320–339 $\Omega/\square$), for *RRR* (0.76–0.82), and for ΔT_c (1.0–1.2 K) for all substrates except hBN. The robustness of the electrical properties is attributed to the film thickness that is considerably larger than the surface roughness.

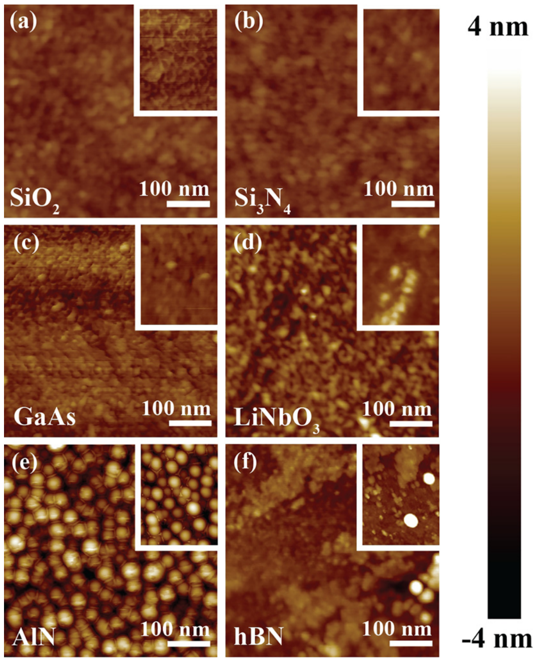

FIG. 1. Atomic force microscopy topography map of NbTiN films (thickness 10 nm) on six different substrates: (a) SiO_2, (b) Si_3N_4, (c) GaAs, (d) $LiNbO_3$, (e) AlN, and (f) hBN. The inset shows a scan of the bare substrates for comparison.

TABLE I. Summary of atomic force microscopy characterization and electrical properties: root mean square surface roughness R_q ($5 \times 5\,\mu$m scan area), room temperature sheet resistance R_{sh}, critical temperature T_c, residual resistance ratio *RRR*, and superconducting transition width ΔT_c.

	$R_{q,substr.}$ (nm)	$R_{q,film}$ (nm)	R_{sh} ($\Omega/\square$)	T_c (K)	*RRR*	ΔT_c (K)
SiO_2	0.5	0.4	339	10.2	0.76	1.0
Si_3N_4	0.3	0.3	320	10.5	0.82	1.1
GaAs	0.6	0.6	335	10.7	0.82	1.1
$LiNbO_3$	0.9	0.9	334	10.4	0.78	1.2
AlN	1.3	1.2	339	11.0	0.76	1.2
hBN	1.2	1.0	239	10.1	0.61	0.8

Interestingly, the properties of NbTiN thin films deposited on a monolayer two-dimensional crystal are different with lower values for R_{sh} ($239\,\Omega/\square$), RRR (0.61), and ΔT_c (0.8 K). On the one hand, the decreased R_{sh} and RRR of the NbTiN thin film could be linked with differences in the nanoscale grain structure, strain, and crystallographic defects.[29] It can be anticipated that the absence of dangling bonds on two-dimensional crystals influences the NbTiN growth mode due to relaxed lattice matching conditions, which is often referred to as van der Waals epitaxy.[30] On the other hand, the reduced superconducting transition width indicates a high level of NbTiN homogeneity on the monolayer hBN substrate. Additional studies will be required to correlate differences in the nanoscale film morphology and/or chemical composition using characterization techniques such as transmission electron microscopy and x-ray photoelectron spectroscopy. Also, it will be interesting to further explore the deposition of NbTiN on different types of two-dimensional crystals in the future.

NbTiN nanostrips were fabricated by means of electron beam lithography (ma-N resist; 50 kV acceleration voltage) and reactive ion etching with fluorine-based gas chemistry. A scanning electron microscopy image of a representative device is shown for the case of the GaAs substrate in Fig. 2(a). A hairpin-shaped nanostrip structure with a width of 100 nm was connected to a series inductor (to reduce the probability of latching[31]) and bonding pads (not shown). The design employing a nanostrip with a single bend is suitable for waveguide-coupled SSPD devices in photonic integrated circuits.[7] NbTiN nanostrip devices were characterized in a closed-cycle cryostat at 2.5 K. V–I measurements were performed using a custom-made battery-powered instrument and an in-line low-pass electrical filter with a cutoff frequency of 1 kHz to determine the critical currents I_c and the retrapping currents I_r [Fig. 2(b)]. Note that the observed resistive slopes are mainly determined by the low-pass filter rather than the normal-state resistance of the NbTiN nanostrips. The measured values for I_c, which showed significant variations in the presented devices, are limited by the current crowding effect in the nanostrip bend,[32,33] by local constrictions and/or imperfections introduced by nanofabrication. Conversely, the values for I_r differed by only about 30%. Hence, the latter parameter, which is often associated with self-heating and thermal sinking,[24,34,35] was found to be rather insensitive to the substrate material.

Furthermore, the devices were operated as SSPDs under flood illumination with photons at a wavelength of 650 nm using commercial readout electronics (Single Quantum B.V.). Normalized photon count rates are presented in Fig. 3(a) as a function of bias current; the comparable sigmoid curve shapes with saturation of the photon count rates indicate internal quantum efficiencies close to unity[36] (except the detector on hBN showing limited saturation). The detection efficiencies were not compared due to the expected variations in photon absorption resulting from the different substrate configurations. From the photon count rate curves, it can be seen that the SSPDs on different substrates had dissimilar dark count characteristics. In particular, the detectors on AlN and hBN (highest surface roughness) exhibited a pronounced onset of dark counts at low currents around $0.9 \cdot I_c$. The evaluation of dark count rates R_{DC} from additional measurements without photon illumination showed that the detectors fabricated on SiO_2 and Si_3N_4 (lowest surface roughness) were particularly suited for operation close to I_c with values for R_{DC} of only a few Hz. These trends suggest that the generation of dark counts via vortex entry induced by

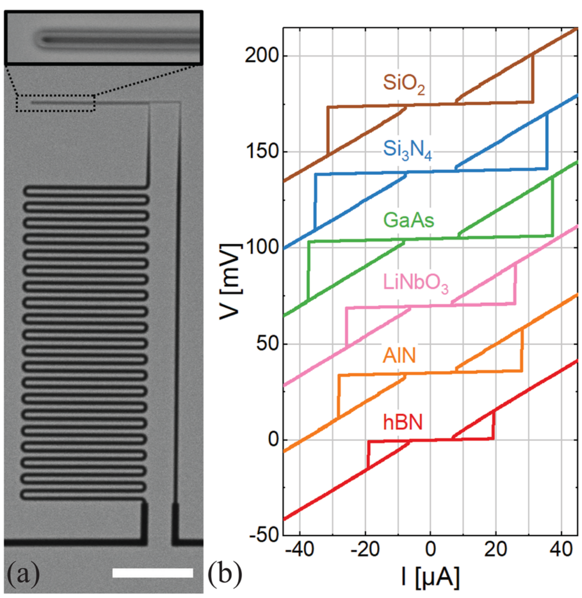

FIG. 2. (a) Superconducting device on the GaAs substrate (scanning electron microscopy image; scale bar 10 μm), which consists of a hairpin-shaped nanostrip structure and a series inductor. The inset shows a magnified view of the hairpin with a nanostrip width of 100 nm. (b) V–I measurements of superconducting nanostrip devices on different platforms (vertical offset for clarity). Positive and negative bias sweeps were performed to characterize the critical current I_c and the retrapping current I_r.

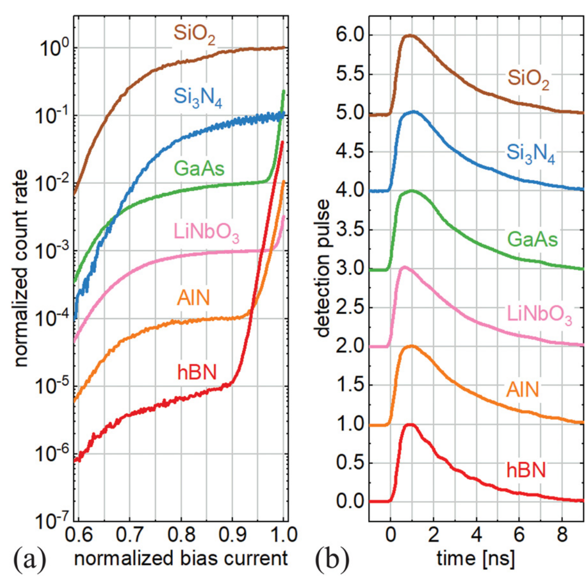

FIG. 3. (a) Normalized photon count rate of superconducting photon detectors on different platforms as a function of bias current (normalized to the critical current I_c). Data were obtained under flood illumination at a wavelength of 650 nm and are displayed with an offset between different devices (factor 10) for clarity. The marked count rate increase close to the critical current I_c is attributed to dark counts. (b) Normalized detection pulses of devices on different platforms (vertical offset for clarity).

TABLE II. Summary of critical currents I_c, retrapping currents I_r, dark count rates R_{DC}, and time constants τ of detector recovery.

	I_c (μA)	I_r (μA)	R_{DC} (Hz)	τ (ns)
SiO_2	31.1	7.8	5.0[a]	2.8
Si_3N_4	35.5	7.7	2.4[a]	2.7
GaAs	37.2	8.5	5.0[b]	2.6
$LiNbO_3$	25.7	6.5	31.8[b]	3.0
AlN	27.8	7.9	125.7[b]	3.1
hBN	19.1	6.7	29.6[b]	2.5

[a]Dark count rate in the range between 0.95 I_c and 0.97 I_c.
[b]Dark count rate evaluated at 0.9 I_c.

thermal or quantum fluctuations[37] is influenced either directly by the type of substrate and/or indirectly by the substrate affecting the film properties and detector fabrication. The detection pulses showed similar kinetics on all six platforms, as can be seen in Fig. 3(b). Detector recovery was fitted to a single-exponential decay, which resulted in similar time constants τ between 2.5 ns and 3.1 ns. The SSPD recovery time constant is determined by the device kinetic inductance and the impedance of the readout electronics;[38] the comparable values of τ for detectors on different substrates indicate similar kinetic inductances of the presented SSPDs. The device parameters I_c, I_r, R_{DC}, and τ are summarized in Table II.

We have presented NbTiN-based SSPD devices integrated on a broad range of materials systems relevant for photonics, including monolayer two-dimensional crystals. High internal quantum efficiencies and comparable detector recovery times were achieved without any further optimization of the universal deposition recipe used for all substrates. Our results demonstrate that reactive co-sputtering of NbTiN at room temperature is a versatile technique to realize superconducting devices for various platforms and applications.

S.S. acknowledges funding from the Swedish Research Council under Grant Agreement No. 2019-04821. S.G. acknowledges funding from the Swedish Research Council under Grant Agreement No. 2016-06122 (Optical Quantum Sensing). K.G. acknowledges funding from the Swedish Research Council (VR, Grant No. 2018-04487). V.Z. acknowledges funding from the European Research Council under Grant Agreement No. 307687 (NaQuOp), the Knut and Alice Wallenberg Foundation (KAW, "Quantum sensors"), and the Swedish Research Council (VR, Grant Nos. 638-2013-7152 and 2018-04251). This project received funding from the European Union's Horizon 2020 research and innovation program under Grant Agreement No. 820423 (S2QUIP).

REFERENCES

[1]G. N. Gol'tsman, O. Okunev, G. Chulkova, A. Lipatov, A. Semenov, K. Smirnov, B. Voronov, A. Dzardanov, C. Williams, and R. Sobolewski, "Picosecond superconducting single-photon optical detector," Appl. Phys. Lett. **79**, 705–707 (2001).
[2]International Electrotechnical Commission, "Superconductivity—Part 22-1: Superconducting electronic devices-generic specification for sensors and detectors," in IEC 61788-22-1 (2017).
[3]I. Holzman and Y. Ivry, "Superconducting nanowires for single-photon detection: Progress, challenges, and opportunities," Adv. Quantum Technol. **2**, 1800058 (2019).
[4]H. Zhang, L. Xiao, B. Luo, J. Guo, L. Zhang, and J. Xie, "The potential and challenges of time-resolved single-photon detection based on current-carrying superconducting nanowires," J. Phys. D **53**, 013001 (2020).
[5]F. Marsili, F. Bellei, F. Najafi, A. E. Dane, E. A. Dauler, R. J. Molnar, and K. K. Berggren, "Efficient single photon detection from 500 nm to 5 μm wavelength," Nano Lett. **12**, 4799–4804 (2012).
[6]F. Marsili, V. B. Verma, J. A. Stern, S. Harrington, A. E. Lita, T. Gerrits, I. Vayshenker, B. Baek, M. D. Shaw, R. P. Mirin, and S. W. Nam, "Detecting single infrared photons with 93% system efficiency," Nat. Photonics **7**, 210–214 (2013).
[7]C. Schuck, W. H. P. Pernice, and H. X. Tang, "Waveguide integrated low noise NbTiN nanowire single-photon detectors with milli-Hz dark count rate," Sci. Rep. **3**, 1893 (2013).
[8]I. Esmaeil Zadeh, J. W. N. Los, R. B. M. Gourgues, V. Steinmetz, G. Bulgarini, S. M. Dobrovolskiy, V. Zwiller, and S. N. Dorenbos, "Single-photon detectors combining high efficiency, high detection rates, and ultra-high timing resolution," APL Photonics **2**, 111301 (2017).
[9]W. Zhang, L. You, H. Li, J. Huang, C. Lv, L. Zhang, X. Liu, J. Wu, Z. Wang, and X. Xie, "NbN superconducting nanowire single photon detector with efficiency over 90% at 1550 nm wavelength operational at compact cryocooler temperature," Sci. China Phys., Mech. Astron. **60**, 120314 (2017).
[10]S. Ferrari, C. Schuck, and W. Pernice, "Waveguide-integrated superconducting nanowire single-photon detectors," Nanophotonics **7**, 1725–1758 (2018).
[11]E. E. Wollman, V. B. Verma, A. E. Lita, W. H. Farr, M. D. Shaw, R. P. Mirin, and S. W. Nam, "Kilopixel array of superconducting nanowire single-photon detectors," Opt. Express **27**, 35279–35289 (2019).
[12]M. Caloz, M. Perrenoud, C. Autebert, B. Korzh, M. Weiss, C. Schönenberger, R. J. Warburton, H. Zbinden, and F. Bussières, "High-detection efficiency and low-timing jitter with amorphous superconducting nanowire single-photon detectors," Appl. Phys. Lett. **112**, 061103 (2018).
[13]L. Redaelli, G. Bulgarini, S. Dobrovolskiy, S. N. Dorenbos, V. Zwiller, E. Monroy, and J. M. Gérard, "Design of broadband high-efficiency superconducting-nanowire single photon detectors," Supercond. Sci. Technol. **29**, 065016 (2016).
[14]R. Gourgues, I. E. Zadeh, A. W. Elshaari, G. Bulgarini, J. W. N. Los, J. Zichi, D. Dalacu, P. J. Poole, S. N. Dorenbos, and V. Zwiller, "Controlled integration of selected detectors and emitters in photonic integrated circuits," Opt. Express **27**, 3710–3716 (2019).
[15]C. Schuck, W. H. P. Pernice, and H. X. Tang, "NbTiN superconducting nanowire detectors for visible and telecom wavelengths single photon counting on Si_3N_4 photonic circuits," Appl. Phys. Lett. **102**, 051101 (2013).
[16]F. Najafi, J. Mower, N. C. Harris, F. Bellei, A. Dane, C. Lee, X. Hu, P. Kharel, F. Marsili, S. Assefa, K. K. Berggren, and D. Englund, "On-chip detection of non-classical light by scalable integration of single-photon detectors," Nat. Commun. **6**, 5873 (2015).
[17]D. Zhu, H. Choi, T.-J. Lu, Q. Zhao, A. Dane, F. Najafi, D. R. Englund, and K. K. Berggren, "Superconducting nanowire single-photon detector on aluminum nitride," in *Conference on Lasers and Electro-Optics* (Optical Society of America, 2016), p. FTu4C.1.
[18]M. G. Tanner, L. S. E. Alvarez, W. Jiang, R. J. Warburton, Z. H. Barber, and R. H. Hadfield, "A superconducting nanowire single photon detector on lithium niobate," Nanotechnology **23**, 505201 (2012).
[19]E. Smirnov, A. Golikov, P. Zolotov, V. Kovalyuk, M. Lobino, B. Voronov, A. Korneev, and G. Goltsman, "Superconducting nanowire single-photon detector on lithium niobate," J. Phys. **1124**, 051025 (2018).
[20]J. P. Höpker, T. Gerrits, A. Lita, S. Krapick, H. Herrmann, R. Ricken, V. Quiring, R. Mirin, S. W. Nam, C. Silberhorn, and T. J. Bartley, "Integrated transition edge sensors on titanium in-diffused lithium niobate waveguides," APL Photonics **4**, 056103 (2019).
[21]F. Marsili, A. Gaggero, L. H. Li, A. Surrente, R. Leoni, F. Lévy, and A. Fiore, "High quality superconducting NbN thin films on GaAs," Supercond. Sci. Technol. **22**, 095013 (2009).
[22]A. Gaggero, S. J. Nejad, F. Marsili, F. Mattioli, R. Leoni, D. Bitauld, D. Sahin, G. J. Hamhuis, R. Nötzel, R. Sanjines, and A. Fiore, "Nanowire

superconducting single-photon detectors on GaAs for integrated quantum photonic applications," Appl. Phys. Lett. **97**, 151108 (2010).
[23]M. Kaniber, F. Flassig, G. Reithmaier, R. Gross, and J. J. Finley, "Integrated superconducting detectors on semiconductors for quantum optics applications," Appl. Phys. B **122**, 115 (2016).
[24]E. Schmidt, K. Ilin, and M. Siegel, "AlN-buffered superconducting NbN nanowire single-photon detector on GaAs," IEEE Trans. Appl. Supercond. **27**, 1–5 (2017).
[25]X. Li, L. Tao, Z. Chen, H. Fang, X. Li, X. Wang, J.-B. Xu, and H. Zhu, "Graphene and related two-dimensional materials: Structure-property relationships for electronics and optoelectronics," Appl. Phys. Rev. **4**, 021306 (2017).
[26]K. Zhang, Y. Feng, F. Wang, Z. Yang, and J. Wang, "Two dimensional hexagonal boron nitride (2D-hBN): Synthesis, properties and applications," J. Mater. Chem. C **5**, 11992–12022 (2017).
[27]J. Zichi, J. Chang, S. Steinhauer, K. von Fieandt, J. W. N. Los, G. Visser, N. Kalhor, T. Lettner, A. W. Elshaari, I. E. Zadeh, and V. Zwiller, "Optimizing the stoichiometry of ultrathin NbTiN films for high-performance superconducting nanowire single-photon detectors," Opt. Express **27**, 26579–26587 (2019).
[28]H. Machhadani, J. Zichi, C. Bougerol, S. Lequien, J.-L. Thomassin, N. Mollard, A. Mukhtarova, V. Zwiller, J.-M. Gérard, and E. Monroy, "Improvement of the critical temperature of NbTiN films on III-nitride substrates," Supercond. Sci. Technol. **32**, 035008 (2019).
[29]P. Patsalas, N. Kalfagiannis, S. Kassavetis, G. Abadias, D. Bellas, C. Lekka, and E. Lidorikis, "Conductive nitrides: Growth principles, optical and electronic properties, and their perspectives in photonics and plasmonics," Mater. Sci. Eng. R **123**, 1–55 (2018).
[30]A. Koma, "Van der Waals epitaxy for highly lattice-mismatched systems," J. Cryst. Growth **201-202**, 236–241 (1999).
[31]A. J. Annunziata, O. Quaranta, D. F. Santavicca, A. Casaburi, L. Frunzio, M. Ejrnaes, M. J. Rooks, R. Cristiano, S. Pagano, A. Frydman, and D. E. Prober, "Reset dynamics and latching in niobium superconducting nanowire single-photon detectors," J. Appl. Phys. **108**, 084507 (2010).
[32]D. Henrich, P. Reichensperger, M. Hofherr, J. M. Meckbach, K. Il'in, M. Siegel, A. Semenov, A. Zotova, and D. Y. Vodolazov, "Geometry-induced reduction of the critical current in superconducting nanowires," Phys. Rev. B **86**, 144504 (2012).
[33]H. L. Hortensius, E. F. C. Driessen, T. M. Klapwijk, K. K. Berggren, and J. R. Clem, "Critical-current reduction in thin superconducting wires due to current crowding," Appl. Phys. Lett. **100**, 182602 (2012).
[34]M. Tinkham, J. U. Free, C. N. Lau, and N. Markovic, "Hysteretic I-V curves of superconducting nanowires," Phys. Rev. B **68**, 134515 (2003).
[35]P. Li, P. M. Wu, Y. Bomze, I. V. Borzenets, G. Finkelstein, and A. M. Chang, "Retrapping current, self-heating, and hysteretic current-voltage characteristics in ultranarrow superconducting aluminum nanowires," Phys. Rev. B **84**, 184508 (2011).
[36]K. Smirnov, A. Divochiy, Y. Vakhtomin, P. Morozov, P. Zolotov, A. Antipov, and V. Seleznev, "NbN single-photon detectors with saturated dependence of quantum efficiency," Supercond. Sci. Technol. **31**, 035011 (2018).
[37]A. Korneev, A. Semenov, D. Vodolazov, G. N. Gol'tsman, and R. Sobolewski, "Physics and operation of superconducting single-photon devices," in *Superconductors at the Nanoscale: From Basic Research to Applications*, edited by R. Wördenweber, V. Moshchalkov, S. Bending, and F. Tafuri (De Gruyter, 2017), Chap. 9, pp. 279–308.
[38]A. J. Kerman, E. A. Dauler, W. E. Keicher, J. K. W. Yang, K. K. Berggren, G. Gol'tsman, and B. Voronov, "Kinetic-inductance-limited reset time of superconducting nanowire photon counters," Appl. Phys. Lett. **88**, 111116 (2006).